MULTIBODY DYNAMICS 2005, ECCOMAS Thematic Conference
J.M. Goicolea, J. Cuadrado, J.C. García Orden (eds.)
Madrid, Spain, 21–24 June 2005

VELOCITY DEPENDENCE OF JOINT FRICTION IN ROBOTIC MANIPULATORS WITH GEAR TRANSMISSIONS

Rob Waiboer[1], Ronald Aarts[2] and Ben Jonker[2]

[1]Netherlands Institute for Metals Research
P.O.Box 5008, 2600 GA Delft, The Netherlands
e-mail: r.r.waiboer@alumnus.utwente.nl

[2]Laboratory of Mechanical Automation
Department of Engineering Technology
University of Twente
P.O. Box 217, 7500 AE Enschede, The Netherlands
e-mails: r.g.k.m.aarts@utwente.nl, j.b.jonker@utwente.nl,
web page: http://www.wa.ctw.utwente.nl

Keywords: Joint friction modelling, helical gear pair, pre-stressed roller bearing, non-linear viscous friction, asperity friction, Stribeck curve, gear transmission, industrial robot.

Abstract. *This paper analyses the problem of modelling joint friction in robotic manipulators with gear transmissions at joint velocities varying from close to zero until their maximum appearing values. It is shown that commonly used friction models that incorporate Coulomb, (linear) viscous and Stribeck components are inadequate to describe the friction behaviour for the full velocity range. A new friction model is proposed that relies on insights from tribological models. The basic friction model of two lubricated discs in rolling-sliding contact is used to analyse viscous friction and friction caused by asperity contacts inside gears and roller bearings of robot joint transmissions. The analysis shows different viscous friction behaviour for gears and pre-stressed bearings. The sub-models describing the viscous friction and the friction due to the asperity contacts are combined into two friction models; one for gears and one for the pre-stressed roller bearings. In this way, a new friction model [1] is developed that accurately describes the friction behaviour in the sliding regime with a minimal and physically sound parametrisation. The model is linear in the parameters that are temperature dependent, which allows to estimate these parameters during the inertia parameter identification experiments. The model, in which the Coulomb friction effect has disappeared, has the same number of parameters as the commonly used Stribeck model [2]. The model parameters are identified experimentally on a Stäubli RX90 industrial robot.*

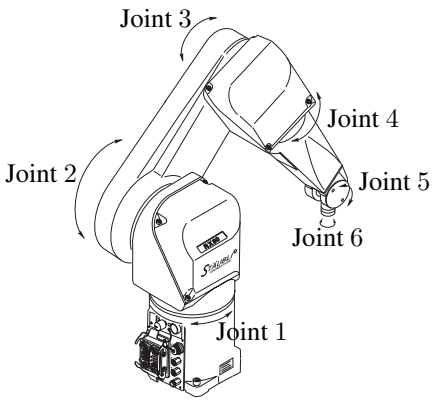

Figure 1: Stäubli RX90B six-axes industrial robot. Courtesy of Stäubli, Faverges, France.

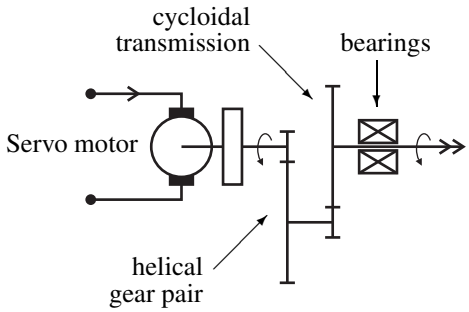

Figure 2: Schematic representation of the gear transmission inside the joint assembly.

1 INTRODUCTION

Experimental identification of the inertia parameters of robotic manipulators imposes high demands on the accuracy of the applied friction models as friction contributes significantly to the measured joint torques. The friction models commonly used in robot literature for this purpose, so called classical friction models, incorporate Coulomb, (linear) viscous and Stribeck components [1]. These models establish that the friction torque is a function of the joint velocity. However, it will be shown in this paper that these models are inadequate to describe the non-linear viscous friction behaviour at high velocities. The models can be improved ad hoc by including extra (non-linear) terms with extra parameters in the friction model, but the physical meaning of such additions is unclear.

This paper analyses the problem of modelling joint friction in industrial robots at velocities varying from close to zero up to the maximum appearing values. In order to get an understanding of friction in the joints of industrial robots, a closer look is taken at the gear transmissions inside the joint assemblies of the Stäubli RX90 robot, see figure 1. The first four joints of the robot, see figure 2, are equipped with a so-called JCS (Stäubli Combined Joint), which is a sophisticated assembly that includes both a cycloidal transmission and the joint bearing support. The cycloidal transmission is driven by a servo motor via a helical gear pair. The gears and bearings in the cycloidal transmission are prestressed in order to eliminate any backlash or play. Both the cycloidal transmission and the helical gear pair are lubricated by means of an oil bath in order to reduce friction losses and to minimise wear. Naturally, all joints are equipped with roller bearings. The remaining two joints in the robot's wrist will not be discussed in this paper as they have a different set-up.

A new friction model is proposed that relies on insights from tribological models. The basic friction model of two lubricated discs in rolling-sliding contact is used to analyse viscous friction and friction caused by asperity contacts inside gears and roller bearings of the robot joints. The sub-models that describe the viscous friction and friction due to the asperities are combined into two friction models: one for gears and one for pre-stressed roller bearings. In this way a new friction model is developed that accurately describes the friction behaviour observed in the Stäubli RX90 industrial robot.

A brief description of the classical friction models and their applicability in industrial robot identification is given in section 2. In section 3, the friction phenomena of a single lubricated contact is discussed on the basis of two lubricated discs in a rolling-sliding contact; expressions for the friction forces due to lubricant viscosity and asperity contacts are presented. These

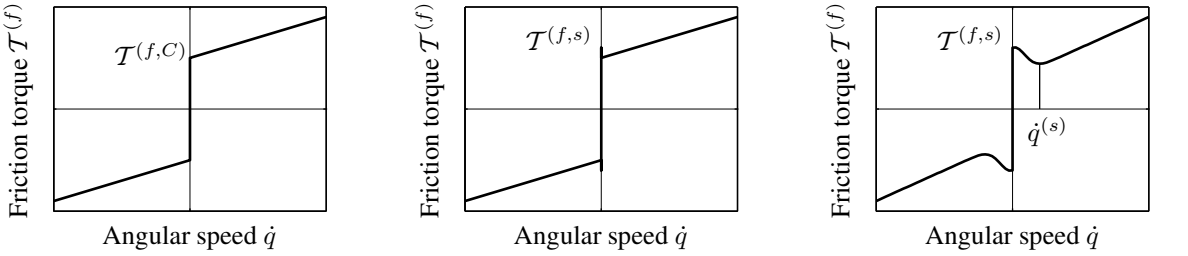

(a) Coulomb & viscous friction, Eq. (2).

(b) Coulomb, viscous and static friction, Eq. (3).

(c) The Stribeck effect, Eq. (5).

Figure 3: Classic friction models.

expressions are applied to model friction forces arising in two typical transmission components like the helical gear pair and the pre-stressed roller bearing in section 4. In section 5 these models are combined into a friction model that accounts for friction in a single joint. The unknown friction parameters of the friction model are identified by means of experiments in section 6. It will be shown that the friction model is linear in the parameters that depend on the temperature of the robot joint, which makes it very suitable to use the friction models in inertia parameter identification experiments.

2 FRICTION MODELLING AT SYSTEM LEVEL

2.1 Classical friction models

Most friction models in robot literature are combinations of the classical friction models, see figure 3. For modelling of friction in robots with revolute joints, friction is usually modelled as a joint torque $\mathcal{T}_j^{(f)}$ which is a function of its angular joint speed $\dot{q}_j$. The subscript j denotes the joint number. The most elementary model is the Coulomb friction model:

$$\mathcal{T}^{(f)} = \operatorname{sign}(\dot{q})\, \mathcal{T}^{(f,C)}\,, \tag{1}$$

where $\mathcal{T}^{(f,C)}$ is the Coulomb friction torque and $\dot{q}$ is the angular speed. The Coulomb friction model originates to the friction between sliding dry surfaces which generally produce large friction forces. Note that $\operatorname{sign}(\dot{q})$ is not defined for zero velocities. This means that the model is not able to describe the friction torque for a velocity equal to zero. The application of a lubricant between the surfaces results in the addition of a viscous term, see figure 3(a), in the friction model:

$$\mathcal{T}^{(f)} = \operatorname{sign}(\dot{q})\, \mathcal{T}^{(f,C)} + c^{(v)}\dot{q}\,, \tag{2}$$

where $c^{(v)}$ is the viscous friction parameter. Viscous friction is, in this model, taken as a linear function of the angular joint speed.

It was found by the Swiss scientist Euler (1707-1783) that a higher force was needed to bring the surfaces in a sliding motion than there is needed to keep the surfaces in motion, see figure 3(b). This so-called static friction effect is taken into account as

$$\mathcal{T}^{(f)} = \begin{cases} |\mathcal{T}^{(f)}| \leq \mathcal{T}^{(f,s)} & \text{if } \dot{q} = 0\,, \\ \operatorname{sign}(\dot{q})\, \mathcal{T}^{(f,C)} + c^{(v)}\dot{q} & \text{if } \dot{q} \neq 0\,, \end{cases} \tag{3}$$

where $\mathcal{T}^{(f,s)}$ is the static friction torque and $\mathcal{T}^{(f,C)} < \mathcal{T}^{(f,s)}$. Note that this model gives a non-unique solution for the coefficient of friction for zero velocities and that it shows discontinuous behaviour in a transition from zero velocity to nonzero velocity.

Stribeck [3] discovered that the drop from static friction to Coulomb friction is not discontinuous for lubricated surfaces but that it is a continuous function of the velocity, see figure 3(c). Therefore, the graph representing the relation between friction and velocity will hereafter be referred to as the Stribeck curve. A well known model describing the Stribeck effect has been developed by Bo and Pavelescu [4], which has an exponentially decrease from the static friction to the Coulomb friction:

$$\mathcal{T}^{(f)} = \mathrm{sign}(\dot{q}) \left(\mathcal{T}^{(f,C)} + (\mathcal{T}^{(f,s)} - \mathcal{T}^{(f,C)}) e^{-\left|\dot{q}/\dot{q}^{(s)}\right|^{\delta}} \right) , \tag{4}$$

where $\dot{q}^{(s)}$ is known as the Stribeck velocity, which indicates the velocity range in which the Stribeck effect is effective. According to [4] the empirical exponent δ ranges from 0.5 to 1 for different material combinations.

Armstrong-Helouvry [5] adopted this Stribeck model and added a viscous term $c^{(v)}\dot{q}$:

$$\mathcal{T}^{(f)} = \mathrm{sign}(\dot{q}) \left(\mathcal{T}^{(f,C)} + (\mathcal{T}^{(f,s)} - \mathcal{T}^{(f,C)}) e^{-\left|\dot{q}/\dot{q}^{(s)}\right|^{\delta}} \right) + c^{(v)}\dot{q} \, . \tag{5}$$

This friction model has been applied by many authors, e.g. [2, 6, 7], for the modelling of sliding friction in robotic systems. In the next section, the applicability of this model in the modelling of joint friction in an industrial robot is investigated. The five unknown parameters, $\mathcal{T}^{(f,C)}$, $\mathcal{T}^{(f,s)}$, $\dot{q}^{(s)}$, δ and $c^{(v)}$, are determined experimentally.

2.2 Stribeck curve measurement

In order to determine the unknown parameters, a Stribeck curve measurement of the first joint of the Stäubli RX90 is carried out. The joint is moved with a trapezoidal velocity profile at different speeds. The values for the joint torques have been averaged along the constant part of the velocity profile in order to reduce noise and position dependent friction effects.

The joint torques are plotted as a function of the joint velocities $\dot{q}$, see figures 4. The joint torque is normalised with the maximum joint torque. The Stribeck effect is clearly visible in the detailed figure 4(b). Note that the Stribeck velocity parameter $\dot{q}^{(s)}$ does not necessarily coincide with the joint speed where the friction torque has its minimum.

The friction model is a non-linear function of two of the unknown parameters, namely $\dot{q}^{(s)}$ and δ. In order to estimate all five parameters at once, one has to rely on non-linear optimisation techniques. It is commonly known that non-linear optimisation techniques may lead to local optima in which non-physical parameter values are found. Non-linear optimisation techniques can be applied successfully in cases for which the model is consistent with the observed behaviour combined with a proper first estimate of the parameter values.

To prevent difficulties with non-linear estimation techniques, a linear least squares optimisation technique is used to obtain the values for the parameters $\mathcal{T}^{(f,C)}$, $\mathcal{T}^{(f,s)}$ and $c^{(v)}$ which are linear in the model. Values for the parameters $\dot{q}^{(s)}$ and δ are selected manually and are assumed to be constant.

In this way the parameters are identified in three steps. In the first step, the parameters for the Stribeck effect $\dot{q}^{(s)}$ and δ have been given a reasonable value. In step two, the remaining

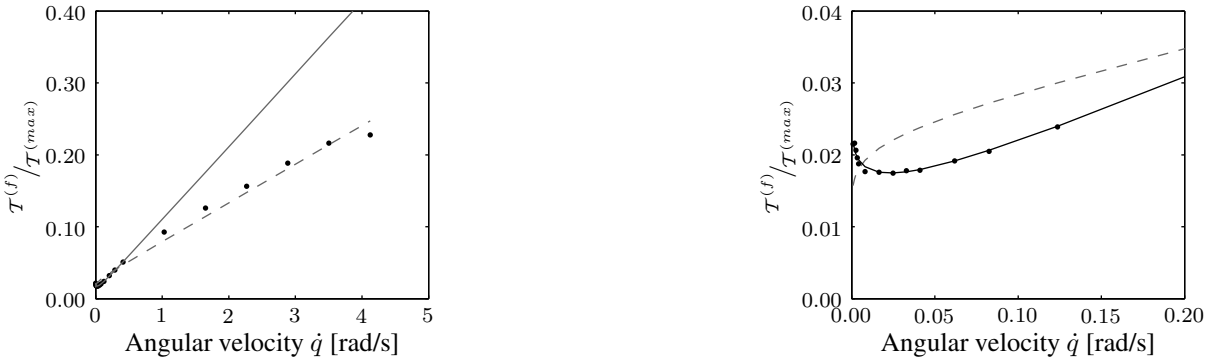

(a) Full velocity range.

(b) Low velocity range.

Figure 4: Stribeck curve for joint 1 of the Stäubli RX90 industrial robot as function of velocity. The dots (•) represent the measurements. Note the non-linear viscous behaviour at high velocities. Model 1 $(--)$ is estimated in the full velocity range whereas model 2 (—) is estimated in the range from 0 to 0.5 rad/s.

parameters $\boldsymbol{p}^{(f)} = \begin{bmatrix} \mathcal{T}^{(f,s)} & \mathcal{T}^{(f,C)} & c^{(v)} \end{bmatrix}^T$ are estimated with a linear least square optimisation, which implies minimising the ℓ^2-norm

$$\hat{\boldsymbol{p}}^{(f)} = \arg\min_{\boldsymbol{p}^{(f)}} \left\| \boldsymbol{\mathcal{T}} - \mathbf{A}^{(f)} \boldsymbol{p}^{(f)} \right\|_2^2 , \tag{6}$$

where $\boldsymbol{\mathcal{T}} = \begin{bmatrix} \mathcal{T}_1 & \cdots & \mathcal{T}_n \end{bmatrix}^T$ is the vector of measured friction torques and matrix $\mathbf{A}^{(f)}$ is defined as

$$\mathbf{A}^{(f)} = \begin{bmatrix} e^{-\left|\dot{q}_1/\dot{q}^{(s)}\right|^\delta} & 1 - e^{-\left|\dot{q}_1/\dot{q}^{(s)}\right|^\delta} & \dot{q}_1 \\ \vdots & \vdots & \vdots \\ e^{-\left|\dot{q}_n/\dot{q}^{(s)}\right|^\delta} & 1 - e^{-\left|\dot{q}_n/\dot{q}^{(s)}\right|^\delta} & \dot{q}_n \end{bmatrix} , \tag{7}$$

for n measured velocity values. The least squares estimates $\hat{\boldsymbol{p}}^{(f)}$ from Eq. (6) can be expressed mathematically as

$$\hat{\boldsymbol{p}}^{(f)} = \left({\mathbf{A}^{(f)}}^T \mathbf{A}^{(f)} \right)^{-1} {\mathbf{A}^{(f)}}^T \boldsymbol{\mathcal{T}} . \tag{8}$$

The last and third step is to fine-tune the manually chosen values for δ and $\dot{q}^{(s)}$. This is an iterative process where the chosen values are changed slightly before the second step is repeated. By inspection of the fit between the modelled Stribeck curve and the measured Stribeck curve the values $\delta = 0.33$ and $\dot{q}^{(s)} = 0.024$ rad/s have been obtained.

In this way, two different parameter sets are estimated; one for the full velocity range from 0 to 4 rad/s and one for a low velocity range from 0 to 0.5 rad/s. As can be observed from figure 4(a), the models 1 and 2 show different behaviour for the low velocity (below 0.5 rad/s) and high velocity (above 0.5 rad/s) range.

Model 1 is estimated for the full velocity range and shows better performance at higher velocities. The low velocity behaviour is clearly not modelled correctly, as a value for the static friction torque is found which is lower than the value for the Coulomb friction. This is caused by the fact that for higher velocities a lower viscous friction parameter shows a better fit. The mismatch for the viscous friction behaviour at low velocity is compensated by a negative Stribeck effect.

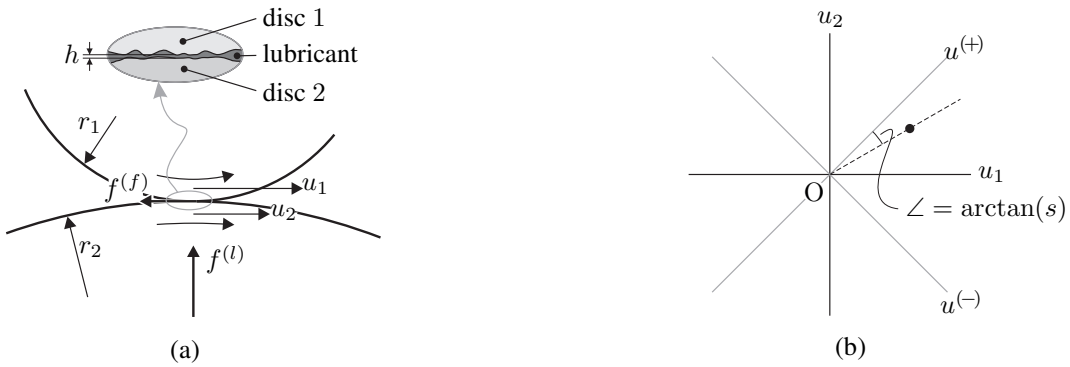

Figure 5: Two lubricated discs in a rolling–sliding contact *(a)* and the velocity diagram *(b)* in which the velocity state ($\bullet$) of a lubricated contact can be indicated.

Model 2 on the other hand shows to be quite accurate for the low velocity range, the Stribeck effect is described accurately, but then the extrapolation into the high velocity range is poor. It appears that linear viscous behaviour of the model in Eq. (5) does not confirm with the actual viscous behaviour of the robot joint.

From the fact that a poor fit is obtained, it can be concluded that the model is not capable to describe the friction phenomena for the full velocity range in the sliding regime. The fit can be improved by including extra (non-linear) terms with extra parameters in the friction model [8], but the physical meaning of such additions in unclear.

3 FRICTION MODELLING AT CONTACT LEVEL

In this section the friction phenomena of a single lubricated contact are studied. On system level, the friction is accounted for as a joint torque $\mathcal{T}^{(f)}$. On contact level, it is more convenient to consider friction as a force $f^{(f)}$. Analogously, the surface velocity u is considered in stead of the joint speed q.

The main components in a robot joint are bearings and gears. In tribology, friction inside gears and bearings is often represented by two lubricated discs in a rolling–sliding contact [9, 10]. The motivation for this representation is that friction in both the roller–raceway contact in roller bearings and the contact between two teeth in a helical or spur gear wheel pair can be represented by the friction behaviour of two lubricated discs in a rolling–sliding contact.

3.1 Two lubricated discs in a rolling–sliding contact

In figure 5(a), an illustration is given of two lubricated discs in a rolling–sliding contact. The friction force between both discs is defined as $f^{(f)}$. The surface velocities of both discs are defined as u_1 and u_2, respectively. The velocity state of the lubricated contact can be expressed as a function of these surface velocities. It is, however, more convenient to express the velocity state of the contact as a function of the sliding velocity and the sum velocity, see the velocity diagram in figure 5(b). The sliding velocity is the difference of both velocities

$$u^{(-)} = u_1 - u_2 \tag{9}$$

and the sum velocity $u^{(+)}$ is defined as

$$u^{(+)} = u_1 + u_2\,. \tag{10}$$

Another frequently used quantity to express the velocity state is the slip ratio s, which is defined as the ratio between the sum and the sliding velocity

$$s = \frac{u^{(-)}}{u^{(+)}} \,. \tag{11}$$

With these definitions, three typical situations for the velocity state can be distinguished:

i. Perfect rolling. Both velocities, u_1 and u_2, are equal in magnitude and direction. Then the sliding velocity $u^{(-)}$ equals zero and, consequently, there is zero slip. This velocity state is indicated by the $u^{(+)}$-axis.

ii. Full sliding. Both velocities, u_1 and u_2, are equal in magnitude and opposite in direction. Then the sum velocity $u^{(+)}$ equals zero, resulting in infinite slip. This velocity state is indicated by the $u^{(-)}$-axis.

iii. Constant slip. The ratio s between the sum and sliding velocity stays constant. This velocity state is indicated by e.g. the dashed line in figure 5(b). In fact, it may be any line that crosses the origin O.

Next, the friction behaviour will be considered as a function of the velocity state. To cover all velocity states it is convenient to consider the friction behaviour at a constant slip ratio, so along the dashed line in figure 5(b). Furthermore, the friction behaviour is considered for varying slip ratios, at a constant sum velocity. This case will be discussed first.

Traction

The friction behaviour as function of the slip ratio s is known as traction. Suppose that one of the discs drives the other disc. The friction force that is needed to bring the second disc in motion is known as the traction force. A typical traction curve is illustrated in figure 6. Note that in a zero slip situation, i.e. in a pure rolling contact, the friction force is zero.

For small slip ratios the traction force–slip ratio has a linear relationship due to Newtonian viscous behaviour of the lubricant. At higher slip ratios the viscous behaviour starts to become non-Newtonian. If the slip ratio is further increased the traction force might start to drop due to shear heating of the lubricant [10]. The traction force is to a large extent determined by the viscous behaviour of the lubricant.

Stribeck behaviour

The friction behaviour as function of velocity at a constant slip ratio is expressed by the Stribeck curve. As the Stribeck curve is defined for a constant slip ratio, the curve may be plotted as a function of either the sum velocity $u^{(+)}$ or the sliding velocity $u^{(-)}$. Schipper [11] defines a lubrication number

$$\mathcal{L} = \frac{\eta_0 u^{(+)}}{p_{\mathrm{av}} R_{\mathrm{a}}} \,, \tag{12}$$

where η_0 is the viscosity, p_{av} is the average pressure and R_{a} is the combined surface roughness. Plotting the Stribeck curve as a function of this lubrication number $\mathcal{L}$ yields a so-called generalised Stribeck curve.

The Stribeck curve is characterised by three lubrication regimes: Boundary Lubrication (BL), Mixed Lubrication (ML) and Elasto-Hydrodynamic Lubrication (EHL). In figure 7, these

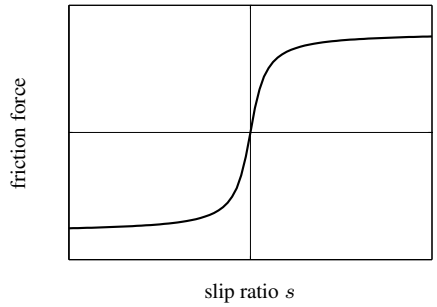

Figure 6: Traction curve: the friction force as a function of varying slip at a constant sum velocity.

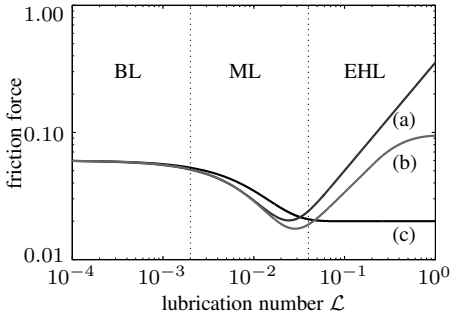

Figure 7: A typical Stribeck curve for an arbitrary lubricated contact as function of the lubrication number $\mathcal{L}$ and for a constant slip ratio s.

lubrication regimes are indicated in a typical Stribeck curve for an arbitrary lubricated contact. In the BL regime, at very low velocity, the friction force is mainly caused by the metallic contact between the surface asperities. The height of the lubricant film between the surfaces is in the same order as the height of the surface summits. As the velocity increases, the lubricant film grows and less asperities are in contact, resulting in a reduction of the friction force caused by the surface summits. On the other hand, viscous friction caused by the lubricant is increasing. This regime is known as the ML regime. Finally, in the EHL regime, the lubricant film has grown such that the surface summits are fully separated. The friction force is the force needed to shear the lubricant film. In figure 7 three different Stribeck curves are plotted. The curves range from full Newtonian behaviour to full non-Newtonian behaviour of the lubricant. Curve *(a)* shows a typical Newtonian behaviour of the lubricant at high velocity. In curve *(b)* the lubricant is mainly Newtonian, but at high velocity the lubricant shows non-Newtonian behaviour. Curve *(c)* corresponds with full non-Newtonian behaviour. It appears that the viscous properties of the lubricant plays a central role in the friction behaviour in the EHL regime.

3.2 Friction force in the lubrication regimes

In the boundary lubrication regime, the friction force is mainly determined by the friction force due to the asperity contacts, denoted by $f^{(a)}$. On the other hand, in the elasto-hydrodynamic lubrication regime, the friction force $f^{(v)}$ due to the viscosity of the lubricating film is dominant. In the mixed lubrication regime both the asperity contacts and the lubricant viscosity determine the total friction force. As a consequence, the total friction force $f^{(f)}$ is assumed to be the sum of the friction force due to the asperity contacts $f^{(a)}$ and a friction force due to the hydrodynamic component $f^{(v)}$ [12]. This leads to the expression for the total friction force

$$f^{(f)} = f^{(a)} + f^{(v)} = \sum_{i=1}^{n^{(a)}} \iint\limits_{A_i^{(a)}} \tau_i^{(a)} \mathrm{d}A_i^{(a)} + \iint\limits_{A^{(H)}} \tau^{(s)} \mathrm{d}A^{(H)} \,, \tag{13}$$

where $n^{(a)}$ is the number of asperities in contact, $A_i^{(a)}$ denotes the area of contact of a single asperity i, $\tau_i^{(a)}$ represents the shear stress at the asperity contact i, $\tau^{(s)}$ is the shear stress of the hydrodynamic component and $A^{(H)}$ is the effective area of contact of the hydrodynamic component. In order to model the total friction force, both the friction force due to the asperity contacts $f^{(a)}$ and the friction force due to hydrodynamic component $f^{(v)}$ need to be investigated.

3.2.1 Friction force due to the hydrodynamic component

The force needed to shear a fluid film resembles the sliding friction between two lubricated surfaces. The fact that a force is needed to shear a fluid film was first proposed by Sir Isaac Newton (1642-1727). Newton states that the shear stress $\tau^{(s)}$ is proportional to the shear rate $\dot{\gamma}$ in the film

$$\tau^{(s)} = \eta\,\dot{\gamma}\,, \tag{14}$$

where η is known as the viscosity. A lubricant behaviour is called Newtonian when the shear stress–shear rate relation is according to Eq. (14) and consequently have a viscosity which is shear rate independent.

Many lubricants, however, show non-Newtonian behaviour at increasing shear rates and show limiting shear stress for high shear rates. The limiting shear stress implies that the lubricant behaves like a plastic solid for high shear rates. The limiting shear strength is a function of temperature and pressure; it increases at higher pressures and at lower temperature. Furthermore, the value of the shear rate at which the viscous–plastic transition occurs increases with a decrease in pressure and an increase in temperature. At high pressures, such as in roller bearings, most lubricants behave as plastic solids at relative low shear rates.

The model presented in [10] is used to describe the shear stress as a function of the shear rate for a full non-Newtonian fluid,

$$\tau^{(s)} = \tau_l^{(s)}\big(1 - e^{-\frac{\eta_0\dot{\gamma}}{\tau_l^{(s)}}}\big)\,, \tag{15}$$

where η_0 the viscosity at reference temperature and pressure and $\tau_l^{(s)}$ is the maximum shear stress. Assuming that the sliding velocity $u^{(-)}$ is a continuous linear function of the height h of the lubricating film and that there is no slip at the interface between the fluid film and the solid surfaces, the shear rate $\dot{\gamma}$ in the lubricating film can be approximated by

$$\dot{\gamma} = \frac{u^{(-)}}{h}\,. \tag{16}$$

With the above relations, equations (14) and (15) and Eq. (16), the friction force $f^{(v)}$ due to the hydrodynamic component can be be approximated by considering a constant average film height h over a certain hydrodynamic area of contact $A^{(H)}$, yielding

$$f^{(v)} = \iint\limits_{A^{(H)}} \tau^{(s)}\mathrm{d}A^{(H)} \approx \tau^{(s)}A^{(H)}\,. \tag{17}$$

For the Newtonian case, substitution of equations (14) and (16) into Eq. (17), yields the following expression for the friction force due to the hydrodynamic component:

$$f^{(v)} = \eta A^{(H)}\frac{u^{(-)}}{h}. \tag{18}$$

For non-Newtonian situations, substitution of equations (15) and (16) into Eq. (17) yields

$$f^{(v)} = A^{(H)}\tau_l^{(s)}\big(1 - e^{-\frac{\eta_0 u^{(-)}}{\tau_l^{(s)}h}}\big)\,. \tag{19}$$

Inspection of the above relations shows a dependency of the hydrodynamic friction force on the height h of the lubricating film. It appears that h strongly depends on the sum velocity $u^{(+)}$, as will be outlined in more detail next.

Height of the lubricating film

The calculation of the lubricant film height has been studied intensively in Elasto–Hydrodynamic Lubrication (EHL) research [13, 14, 9, 15, 16]. It was found that the film height depends on six independent variables:

R	the radius of the roller pair,	E	the elastic modulus of a roller pair,
η_0	the viscosity,	w	the load per unit width,
α	the pressure exponent of the lubricant; $\eta = \eta_0 e^{\alpha p}$, with pressure p,	$u^{(+)}$	the sum velocity.

The film height is then expressed as a function:

$$\frac{h}{R} = f\left(\frac{w}{ER}, \frac{u^{(+)}\eta_0}{ER}, \alpha E\right) , \tag{20}$$

where the above variables are grouped into four dimensionless parameters. These dimensionless parameters are:

$H = \frac{h}{R}$	the relative film height,	$W = \frac{w}{ER}$	the load parameter,
$U = \frac{u^{(+)}\eta_0}{ER}$	the velocity parameter,	$G = \alpha E$	the material parameter.

It has been found analytically by Dowson and Higginson [9] that the minimum film thickness can fairly accurate be represented by

$$H_{\min} = \frac{1.6 G^{0.6} U^{0.7}}{W^{0.13}} . \tag{21}$$

The equation shows that the influence of the material parameter G is quite large. However, G can be considered as constant for a specific combination of materials and lubricant. Furthermore, the relations show that the load parameter W only weakly influences the film height. The velocity parameter U is clearly the most significant parameter. From expression (21) follows a proportionality between the film height and the sum velocity, expressed as

$$h \propto (u^{(+)})^{0.7} . \tag{22}$$

However, according to experimental results by Crook [14], the film height shows a proportionality to the sum velocity $u^{(+)}$ given by

$$h \propto (u^{(+)})^{0.5} . \tag{23}$$

This indicates that the power in which the film height relates to the sum velocity is not uniquely, but that it varies between 0.5 and 0.7 depending on the details of the specific contact. Therefore, it has to be determined for the specific application at hand.

With these observations, it is possible to express the film height h as a function of the sum velocity $u^{(+)}$ as

$$h = h^{(s)} \left(\frac{u^{(+)}}{u^{(s)}}\right)^{\delta} , \tag{24}$$

where the proportionality constant $h^{(s)}$ represents the reference film height, which is a function of the load parameter W, the material parameter G and the radius R. In order to keep proper

dimension, a scaling velocity $u^{(s)}$ is introduced, which relates to the lubricant viscosity η, the elastic modulus E and the radius R. From equations (22) and (23) it follows that the power δ can range from 0.5 to 0.7.

In this section, a simplified expression for the height of the lubricant film is derived. With this expression and the equations for the viscous friction forces derived in section 3.2.1, the viscous friction force $f^{(v)}$ can be described as function of both the sum $u^{(+)}$ velocity and the sliding velocity $u^{(-)}$. The film height of the lubricant also plays a significant role in the friction force due to the asperity contacts.

3.2.2 Friction force due to asperity contacts

In this section, a relation for the friction force due to the asperity contacts in the boundary lubrication regime will be derived. The normal load acting on a lubricated contact is shared between the hydrodynamic component and the interacting asperities of the surfaces. So as the hydrodynamic action increases as function of the film height, the load carried by the asperities decreases. Greenwood and Williamson [17] introduced an approach to the modelling of the friction caused by the asperities which is based on the statistics of the surface roughness of the surfaces in contact. The height distribution of the surface summits can be considered to be Gaussian, but, according to Greenwood and Williamson [17], an exponential distribution shows to be a fair approximation for the uppermost 25% of the asperities of most surfaces. Using the exponential distribution gives the advantage that a fairly simple expression for the number of asperities $n^{(a)}$ in contact can be used. The expression is given by [17]

$$n^{(a)} = d^{(a)} A^{(a)} \, e^{-\lambda^{(s)}} \,, \tag{25}$$

where $d^{(a)}$ is the asperity density and $A^{(a)}$ the total area of contact. Exponent $\lambda^{(s)}$ is known as the separation which is the ratio between the film height h and the standard deviation of the height of the surface summits $\sigma^{(s)}$, defined as

$$\lambda^{(s)} = \frac{h}{\sigma^{(s)}} \,. \tag{26}$$

Using the relation for the film height of Eq. (24), the separation can be written as a function of the sum velocity $u^{(+)}$

$$\lambda^{(s)} = \frac{h^{(s)}}{\sigma^{(s)}} \left(\frac{u^{(+)}}{u^{(s)}} \right)^{\delta} \,. \tag{27}$$

The total friction force due to all $n^{(a)}$ asperities can be approximated as

$$f^{(a)} = \sum_{i=1}^{n^{(a)}} \iint\limits_{A_i^{(a)}} \tau_i^{(a)} \mathrm{d}A_i^{(a)} \approx n^{(a)} f^{(a,0)} \,, \tag{28}$$

where $f^{(a,0)}$ is the average force needed to break a single asperity i.

Substitution of expression (25) and Eq. (27) into Eq. (28) yields the expression for the friction force $f^{(a)}$ due to the asperity contacts as a function of the sum velocity

$$f^{(a)} = f^{(a,0)} d^{(a)} A^{(a)} \, \exp\left(-\frac{h^{(s)}}{\sigma^{(s)}} \left(\frac{u^{(+)}}{u^{(s)}} \right)^{\delta} \right) \,. \tag{29}$$

Note the correspondence of Eq. (29) with the model presented by Bo and Pavelescu [4], Eq. (4).

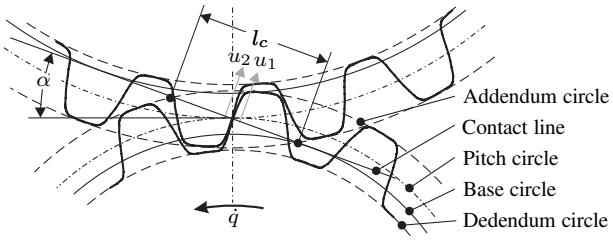

Figure 8: Schematic representation of a gear pair.

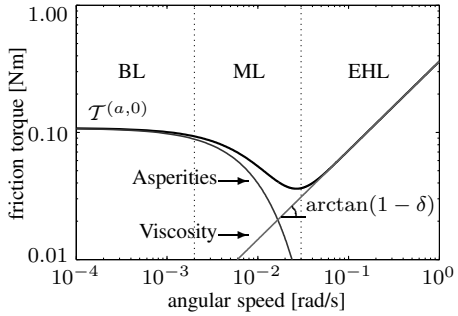

Figure 9: A typical Stribeck curve for a gear pair.

4 FRICTION MODELS OF ELEMENTARY TRANSMISSION COMPONENTS

In sections 3.2.1 and 3.2.2, expressions for the friction force due to lubricant viscosity and due to the asperities for a lubricated contact between two rolling–sliding discs have been presented. In this section, these expressions are applied to model the friction forces arising in the two elementary components; a helical gear-pair and a pre-stressed roller bearing.

4.1 Friction model of a helical gear pair

In figure 8 a schematic representation of a helical gear pair is depicted. Here, the lower gear wheel drives the upper gear wheel. The kinematics associated with a helical gear pair is quite complex. Furthermore, several teeth are in contact at the same instance in a gear pair. As the gear pair is of the helical type, a single teeth is in contact over the full width of the gear wheel along a large part of the contact line l_c.

The two surface velocities u_1 and u_2 have been depicted in the teeth contact illustrated in the figure 8. At the point where the contact line l_c crosses the pitch circle the velocities are equal in magnitude (and direction) which results in a pure rolling motion ($u^{(-)} = 0$). However, at all other points along the contact line, the velocities are not equal in magnitude, leading to a nonzero sliding velocity. At the moment of interconnection of the teeth, the surface velocity u_1 associated with the driving gear is lower in magnitude compared with u_2. Towards the pitch circle they become gradually equal in magnitude. After the moment of pure rolling, u_1 gets larger in magnitude compared with u_2. Consequently, there is a large part during the interconnecting phase where there is a nonzero sliding velocity.

Due to the fact that the power is mainly transferred at the moment of rolling, the contact pressures in a helical gear pair are sufficiently low in order to allow the assumption that the lubricant behaviour will be Newtonian. Consequently, the expression for the viscous friction, Eq. (18), derived in section 3.2.1, will be applied. The film height is highly dependent on the sum velocity, as was shown in section 3.2.1. So substitution of the expression for the film height, Eq. (24), into Eq. (18) yields the viscous friction force for Newtonian behaviour of the lubricant

$$f^{(v)} = \frac{\eta A^{(H)} u^{(-)}}{h^{(s)}} \left(\frac{u^{(s)}}{u^{(+)}} \right)^{\delta}. \tag{30}$$

According to Eq. (13), summation of the viscous friction force, Eq. (30) and the friction force due to the asperities, Eq. (29), leads to the combined friction force in a single teeth contact

$$f^{(f)} = f^{(a)} + f^{(v)} f^{(a,0)} d^{(a)} A^{(a)} \exp\left(-\frac{h^{(s)}}{\sigma^{(s)}} \left(\frac{u^{(+)}}{u^{(s)}} \right)^{\delta} \right) + \frac{\eta A^{(H)} u^{(-)}}{h^{(s)}} \left(\frac{u^{(s)}}{u^{(+)}} \right)^{\delta}. \tag{31}$$

The next step is to derive an expression for the total joint friction torque that is caused by the friction in a gear pair as function of the joint speed $\dot{q}$. Expressing the sum velocity $u^{(+)}$ at a single teeth contact as function of the angular position and velocity of the joint yields a complex geometric function

$$u^{(+)} = f(q, \dot{q})\,. \tag{32}$$

This expression can be simplified by considering a time and position averaged sum velocity $\overline{u}^{(+)}$ for a single teeth pair along the interconnecting phase, yielding

$$\overline{u}^{(+)} = r\dot{q}\,, \tag{33}$$

where r may be considered as a kinematic constant. Analogously, a time and position averaged slip ratio $s_0 = \frac{\overline{u}^{(-)}}{\overline{u}^{(+)}}$ is considered, which yields

$$\overline{u}^{(-)} = s_0 r\dot{q}\,. \tag{34}$$

The total friction torque $\mathcal{T}^{(f)}$ can be derived by multiplying of the averaged friction force $\overline{f}^{(f)}$ with constant r and the number of teeth k in contact. Accordingly, substitution of the equations (33) and (34) for the averaged sum and sliding velocity, respectively, yields the expression for the friction torque of a helical gear pair

$$\mathcal{T}^{(f)}_{gear} = \mathcal{T}^{(a)} + \mathcal{T}^{(v)} = \underbrace{\mathcal{T}^{(a,0)}\, e^{-\left(\dot{q}/\dot{q}^{(s)}\right)^{\delta}}}_{asperities} + \underbrace{c^{(v)}\dot{q}^{(1-\delta)}}_{viscosity}\,. \tag{35}$$

with the parameters

$$\mathcal{T}^{(a,0)} = rkf^{(a,0)}d^{(a)}A^{(a)}\,, \quad \dot{q}^{(s)} = \frac{u^{(s)}}{r}\left(\frac{\sigma^{(s)}}{h^{(s)}}\right)^{1/\delta}\,, \quad c^{(v)} = \frac{r^2 k s_0 \eta A^{(H)}}{h^{(s)}}\left(\frac{u^{(s)}}{r}\right)^{\delta}. \tag{36}$$

A typical Stribeck curve for a helical gear pair, computed by the model in Eq. (35) with an arbitrary parameter set, is illustrated in figure 9. The contributions to the friction torque from both the asperity contacts and the hydrodynamic component are also depicted. It shows clearly that the asperity contacts are responsible for the friction force in the BL regime and that the hydrodynamic component dominates the friction force in the EHL regime.

4.2 Friction model of a pre-stressed roller bearing

In figure 10, a single lubricated roller bearing is illustrated. The bearing is a assembly of two concentric circular raceways, the inner ring and the outer ring. The difference in velocity between the inner ring and the outer ring is covered by the rolling of the rollers in between these raceways. Small differences between the velocities (u_1, u_2), and also between the velocities (u_1', u_2') cause friction forces in the contact surfaces between a roller and both the inner and outer rings. These friction forces form a torque that brings the roller in motion. This process is known as traction, as was introduced in section 3.1. Since the bearing is highly pre-stressed the lubricant behaviour will be non-Newtonian, even for small slip ratios [18].

The friction force can be computed as the sum of the viscous friction and the friction force caused by the asperities. Due to the non-Newtonian behaviour of the lubricant in the bearing, Eq. (19) is used to compute the viscous friction force. Equation (29) will account for the friction

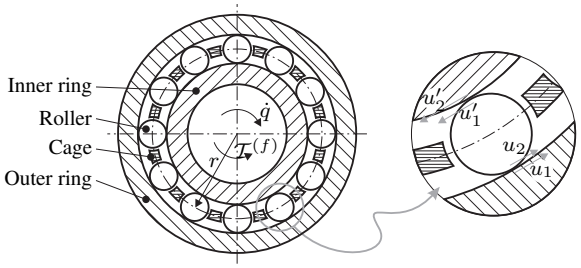

Figure 10: Schematic representation of a roller bearing.

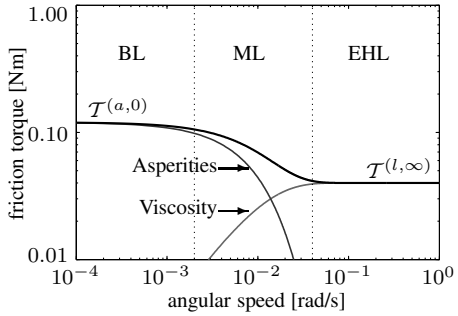

Figure 11: A typical Stribeck curve for a pre-stressed roller bearing.

force due to the asperity contact. Combining these equations yields an expression for the friction force in a single contact between a roller and a raceway inside a bearing

$$f^{(f)} = f^{(a)} + f^{(v)} = f^{(a,0)} d^{(a)} A^{(a)} \, e^{-\frac{h^{(s)}}{\sigma^{(s)}} \left(\frac{u^{(+)}}{u^{(s)}}\right)^{\delta}} + A^{(H)} \tau_l^{(s)} \left(1 - e^{-\frac{\eta_0 u^{(-)}}{\tau_l^{(s)} h}}\right) . \tag{37}$$

The velocities $u^{(+)}$ and $u^{(-)}$ are expressed as functions of the angular joint speed $\dot{q}$ according to

$$u^{(+)} \approx r\dot{q} \, , \qquad\qquad u^{(-)} \approx r s_0 \dot{q} \, , \tag{38}$$

where a constant slip ratio s_0 is assumed and r is the average raceway radius, see Fig. 10.

The total friction torque $\mathcal{T}^{(f)}$ generated by a prestressed roller bearing is considered as the sum of all torques generated by the friction forces at all roller–raceway contacts, which is achieved by multiplying the friction force in Eq. (37) with radius r and the number of rolling elements k. Substitution of the velocity expressions (38) into Eq. (37) yields the expression for the friction torque of a pre-stressed roller bearing

$$\mathcal{T}^{(f)}_{bearing} = \mathcal{T}^{(a)} + \mathcal{T}^{(v)} = \underbrace{\mathcal{T}^{(a,0)} \, e^{-\left(\dot{q}/\dot{q}^{(s)}\right)^{\delta}}}_{asperities} + \underbrace{\mathcal{T}^{(l,\infty)} \left(1 - e^{-\dot{q}/\dot{q}^{(l)}}\right)}_{viscosity} . \tag{39}$$

with the parameters

$$\mathcal{T}^{(a,0)} = r k f^{(a,0)} d^{(a)} A^{(a)} \, , \qquad\qquad \dot{q}^{(s)} = \frac{u^{(s)}}{r} \left(\frac{\sigma^{(s)}}{h^{(s)}}\right)^{1/\delta} \, , \tag{40a}$$

$$\mathcal{T}^{(l,\infty)} = r k \tau_l^{(s)} A^{(H)} \, , \qquad\qquad \dot{q}^{(l)} = \frac{\tau_l^{(s)} h_l}{r s_0 \eta_0} \, . \tag{40b}$$

A typical Stribeck curve for an arbitrary prestressed roller bearing represented by the model in Eq. (39) is illustrated in figure 11. The curves for the friction torque generated by the asperity contacts and the friction torque due to lubricant viscosity are also plotted. Note that the friction torque decreases from the static friction torque $\mathcal{T}^{(a,0)}$ towards the (limiting shear stress) viscous friction torque $\mathcal{T}^{(l,\infty)}$.

The film height h is not included as a function of the rolling velocity in the expression for the viscous friction force in Eq. (39). This simplification is introduced since the dependency of the film height on the rolling velocity only influences the shape of the exponential function associated with the non-Newtonian behaviour. Furthermore, in the velocity region where the

exponential function has an effect, the friction torque is dominated by the friction torque due to the asperity contacts. Therefore, the film height h for the viscous part can in this case be approximated by a constant film height h_l.

In the sections 4.1 and 4.2, friction models for both a gear pair and a prestressed roller bearing have been derived. The models are based on physical models from tribology literature in which elementary variables such as lubricant viscosity, contact topology and material properties have been taken into account. These elementary variables have been combined into a new set of parameters, some of which are constant for a specific contact, while others may change during operation, e.g. due to temperature variations. The number of model parameters is the minimal number that is required to describe the Stribeck behaviour associated with the modelled transmission component. With the derived models it has been shown that it is possible to describe Stribeck curves for both the gear pair and the pre-stressed roller bearing and that they agree well with Stribeck curves presented in literature, e.g. Gelinck and Schipper [12]. In the next section the two models will be used to construct joint friction models for the Stäubli RX90.

5 THE JOINT FRICTION MODEL

The next step is to combine the sub-models that have been derived in the previous section into friction models that account for the friction that arises in a single robot joint. The joint friction model can be considered to be a combination of the friction models associated with the joint transmission components. However, summation of all sub-models will lead to a large friction model which includes many parameters. Instead, only the friction characteristics of the components will be evaluated and only the most significant effects will be taken into account.

The first four robot joints are constructed according to the schematic representation given in figure 2. The assembly contains three main components: a helical gear pair, a cycloidal transmission and the joint bearings. The joint bearings are highly pre-stressed and therefore it is expected that the bearings are responsible for the main part of the asperity friction torque.

The viscous friction torque of the bearings, however, is much lower than its asperity friction torque, as can be observed from the Stribeck curve of the roller bearing, figure 11. Taking into account that the helical gear pair in the joint is operating at a high angular velocity due to the high transmission ratio, it can be expected that its viscous friction torque will be dominant with respect to the viscous friction torque of the bearing.

The cycloidal gears are operating at a low angular velocity and are prestressed as well. This will results in a small viscous friction torque in comparison with the helical gear pair. Furthermore, the friction behaviour at low velocity will be similar to the asperity friction behaviour of a roller bearing.

The final joint friction model will be a combination of the asperity part of the model of a roller bearing, Eq. (39), and the viscous part of the model model of a helical gear pair, Eq. (35). This yields then the combined friction model for joint j:

$$\mathcal{T}_j^{(f)} = \mathcal{T}_j^{(a,0)} e^{-\left(\dot{q}_j/\dot{q}_j^{(s)}\right)^{\delta_j^{(a)}}} + c_j^{(v)} \dot{q}_j^{\left(1-\delta_j^{(v)}\right)} . \tag{41}$$

Note the different values for $\delta_j^{(a)}$ and $\delta_j^{(v)}$ as the friction torque from the asperities and the viscous friction torque are generated at different elements and may therefore show a different film height–velocity behaviour.

For each joint j, there are five unknown parameters; the static asperity friction torque $\mathcal{T}_j^{(a,0)}$, the Stribeck velocity $\dot{q}_j^{(s)}$, the Stribeck velocity power $\delta_j^{(a)}$, the viscous friction coefficient $c_j^{(v)}$ and $\delta_j^{(v)}$ denotes the viscous friction power. The values for these unknown parameters will be obtained by means of experimental identification.

Comparing the friction model in Eq. (41) with the "classical" friction model of [5] as presented in equation (5), two main differences can be noticed. The first difference is shown in the viscous friction part, where the new model shows a non-linear velocity–viscous friction relation in terms of $c^{(v)}\dot{q}^{(1-\delta)}$, as opposed to a linear velocity relation expressed by $c^{(v)}\dot{q}$. The second item in which the new model differs from the standard model is that the Coulomb friction term has disappeared. This is due to the fact that the new friction model is based on lubricated surfaces and that Coulomb friction generally is associated with dry contacts.

6 FRICTION PARAMETER ESTIMATION

The values of the parameters are estimated based on the measured values of the Stribeck curve. The measured values are the mean friction torques at constant joint velocity. Three measurements series will be used in which the measurements at each robot joint are carried out after an initial warmup motion of the robot.

All friction models are nonlinear functions of the parameters $\delta^{(a)}$, $\dot{q}^{(s)}$ and $\delta^{(v)}$, and linear functions of the temperature dependent parameters $\mathcal{T}^{(a,0)}$ and $c^{(v)}$. Estimating these parameters in a single optimisation requires a non-linear optimisation technique. However, non-linear optimisation techniques may lead to local optima in which non-physical parameter values have been found, as was already concluded in section 2.2. To prevent difficulties with non-linear estimation techniques, the values are obtained in four steps by means of linear least squares techniques. These four steps are concisely described below. For a more detailed description of the identification steps, the reader is referred to [1].

The first step of the identification process is to determine the power $1 - \delta^{(v)}$ and the magnitude $c^{(v)}$ of the viscous part. Recall from section 3.2.1 that the power $\delta^{(v)}$ depends on the configuration of the contacts. Because the configuration is assumed to be time invariant, the power $\delta^{(v)}$ has to be determined only once. Taking the natural logarithms of the joint torques and the joint velocities allows for the application of a linear least squares estimation technique to find the viscous friction parameters. Since only the high velocity region, from 0.5 to 4.5 rad/s, is considered, the influence of the asperity friction torques can be neglected.

The second step involves the selection of a proper value for the power $\delta^{(a)}$. As a logical fist estimate, it is set to the same value as $\delta^{(v)}$. Additionally, a value for the Stribeck velocity $\dot{q}^{(s)}$ needs to be chosen. A good first estimate is a value close to the joint speed where the friction torque is at its minimum.

In the third step, the magnitude of the static asperity friction torque $\mathcal{T}^{(a,0)}$ is determined by means of a linear least squares estimation analogue to the estimation technique described in section 2.2. For best model fits, the magnitude of the viscous friction $c^{(v)}$ will again be included in the estimation, which can be done because $c^{(v)}$ is linear in the model.

During the fourth and final step, the manually chosen values for $\delta^{(a)}$ and $\dot{q}^{(s)}$ are manually fine-tuned in an iterative process. The fit between the modelled Stribeck curve and the measured Stribeck curve is inspected visually and by modifying the values for $\delta^{(a)}$ and $\dot{q}^{(s)}$, a set of appropriate vales is obtained.

Figure 12 shows the measured mean Stribeck curve $\overline{\mathcal{T}}^{(f)}$ as well as the estimated Stribeck curve. Note that the measured Stribeck is averaged over $N = 3$ measurements. In figure 12(a)

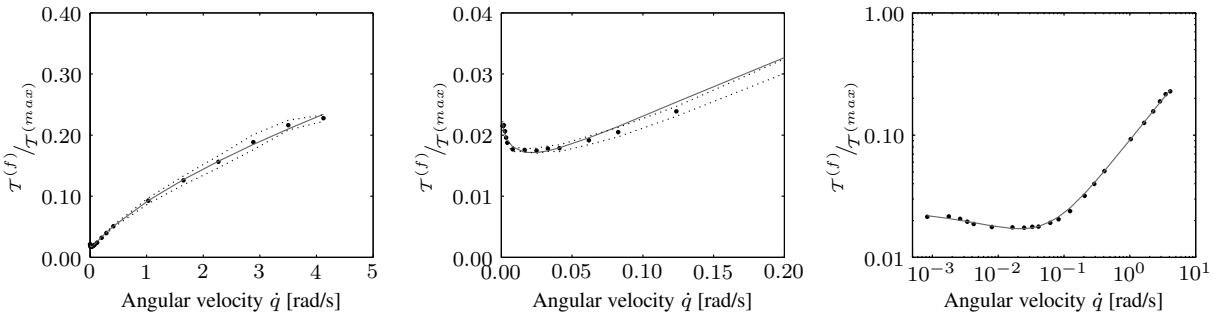

(a) Full velocity range. (b) Low velocity range. (c) Logarithmic scales.

Figure 12: Measured (•) and modelled (—) Stribeck curve for joint 1. The sample standard deviation s of the measured values is indicated by $(\cdots)$.

the full velocity range is shown and in figure 12(b) a detail of the low (Stribeck) velocity range is shown. In both figures also the sampled standard deviation s of the measurements is also plotted. In figure 12(c), both the measured and modelled Stribeck curves for joint 1 are plotted on logarithmic scales. It shows that the relative errors between the model and the measurement are equally small across the full velocity range. Consequently, the model accurately describes both the low and the high velocity range.

7 CONCLUSIONS

In this paper it is shown that classical friction models, commonly used in robot literature, are inadequate to model the viscous friction behaviour for the full velocity range with sufficient accuracy. Therefore, a new joint friction model is developed that relies on insights from sophisticated tribological models. The basic friction model of two lubricated discs in a rolling–sliding contact is used to analyse the different contacts inside the gears and bearings of the robot joint transmissions.

It is shown that the film height of the lubricant is a function of the rolling velocity, which causes a non-linear relation between the joint angular speed and the viscous friction torques. The analysis shows different behaviour for gears and pre-stressed bearings. Furthermore, it is shown that friction torques caused by the asperity contacts depend on the ratio between lubricant film height and the height distribution of the surface summits. Increasing the joint velocity leads to a decrease of the asperity friction torque.

Sub-models for the viscous friction and the friction due to the asperity contacts are combined into two friction models; one for gears and one for prestressed roller bearings. The sub-models describing the asperity part of the roller bearings and the viscous friction part of the helical gear pair are combined into a joint friction model. In this way, a new friction model is developed that accurately describes the friction behaviour in the sliding regime with a minimal and physically sound parametrisation.

The model is linear in the parameters that are temperature dependent, which allows to estimate these parameters during the inertia parameter identification. The model, in which the Coulomb friction effect has disappeared, has exactly the same number of unknown parameters as the commonly used Stribeck model [2].

8 ACKNOWLEDGMENT

This work was carried out under the project number MC8.00073 in the framework of the Strategic Research programme of the Netherlands Institute for Metals Research in the Netherlands (http://www.nimr.nl/).

The authors which to thank Stäubli Faverges, France for the support of the research.

REFERENCES

[1] Waiboer, R. R., to be published in 2005. "Dynamic modelling, identification and simulation of industrial robots for off-line programming of robotised laser welding". PhD thesis, University of Twente, Enschede, The Netherlands.

[2] Canudas De Wit, C., Olsson, P., Aström, K., and Lischinsky, P., 1995. "A new model for control of systems with friction". *IEEE Transactions on Automatic Control,* **40**(3), pp. 419–425.

[3] Stribeck, R., 1902. "Die wesentlichen eigenschaften der gleit- und rollenlager". *Zeitschrift Des Vereines Deutcher Ingenieure,* **46**(38, 39), pp. 1342–1348,1432–1437.

[4] Bo, L. C., and Pavelescu, D., 1982. "The friction–speed relation and its influence on the critical velocity of the stick–slip motion". *Wear,* **82**(3), pp. 277–289.

[5] Armstrong-Hélouvry, B., 1991. *Control of Machines with Friction*. Kluwer Academic Publishers.

[6] Olsson, H., Åström, K. J., Canudas de Wit, C., Gäfvert, M., and Lischinsky, P., 1998. "Friction models and friction compensation". *European Journal of Control,* **4**(3), pp. 176–195.

[7] Hensen, R. H. A., Van de Molengracht, M. J. G., and Steinbuch, M., 2002. "Frequency domain identification of dynamic friction model parameters". *IEEE Transactions on Control Systems Technology,* **10**(2), pp. 191–195.

[8] Grotjahn, M., 2003. "Kompensation nichtlinearer dynamischer effecte bei seriellen und parallelen robotern zur erhöhnung der bahngenauigkeit.". PhD thesis, Universität Hannover.

[9] Dowson, D., and Higginson, G. R., 1977. *Elasto-Hydrodynamic Lubrication*. Pergamon Press Ltd., Oxford.

[10] Bhushan, B., 1999. *Principles and Applications of Tribology*. John Wiley & Sons, New York.

[11] Schipper, D., 1988. "Transitions in the lubrication of concentrated contacts". PhD thesis, University of Twente, Enschede, The Netherlands.

[12] Gelinck, E. R. M., and Schipper, D. J., 2000. "Calculation of stribeck curves for line contacts". *Tribology International,* **33**, pp. 175–181.

[13] Grubin, A. N., and Vinogradova, I. E., 1949. Central scientific research institute for technology & mechanical engineering. Book No. 30 (D.S.I.R Translation No.337).

[14] Crook, A. W., 1961. "The lubrication of rollers II. film thickness with relation to viscosity and speed". *Philosophical Transactions of the Royal Society of London. Series A, Mathematical and Physical Sciences,* **254**(1040), pp. 223–236.

[15] Dowson, D., 1995. "Elastohydrodynamic and micro-elastohydrodynamic lubrication". *Wear,* **190**(2), pp. 125–138.

[16] Spikes, H. A., 1999. "Thin films in elastohydrodynamic lubrication: The contribution of experiment". *Proceedings of the Institution of Mechanical Engineers - J,* **213**(5), pp. 335–352.

[17] Greenwood, J. A., and Williamson, J. B. P., 1966. "Contact of nominally flat surfaces". *Proceedings of the Royal Society of London. Series A, Mathematical and Physical Sciences,* **295**(1442), pp. 300–319.

[18] Bair, S., and Winer, W. O., 1979. "Shear strength measurements of lubricants at high pressure". *ASME Journal of Lubrication Technology,* **101**, pp. 251–257.